Inorganic Chemistry

ARTICLE

pubs.acs.org/IC

Multireversible Redox Processes in Pentanuclear Bis(Triple-Helical) Manganese Complexes Featuring an Oxo-Centered triangular $\{Mn^{II}_2Mn^{III}(\mu_3\text{-}O)\}^{5+}$ or $\{Mn^{II}Mn^{III}_2(\mu_3\text{-}O)\}^{6+}$ Core Wrapped by Two $\{Mn^{II}_2(bpp)_3\}^{-}$

Sophie Romain,[†] Jordi Rich,[‡] Cristina Sens,[‡] Thibaut Stoll,[§] Jordi Benet-Buchholz,[†] Antoni Llobet,[*,†,∥] Montserrat Rodriguez,[*,‡] Isabel Romero,[*,‡] Rodolphe Clérac,[⊥,#] Corine Mathonière,[¶] Carole Duboc,[§] Alain Deronzier,[§] and Marie-Noëlle Collomb[*,§]

[†]Institute of Chemical Research of Catalonia (ICIQ), Av. Països Catalans 16, E-43007 Tarragona, Spain

[‡]Departament de Química, Universitat de Girona and Serveis Tecnics de Recerca, Campus de Montilivi, E-17071 Girona, Spain

[§]Université Joseph Fourier Grenoble 1/CNRS, Département de Chimie Moléculaire, UMR-5250, Laboratoire de Chimie Inorganique Redox, Institut de Chimie Moléculaire de Grenoble FR-CNRS-2607, BP-53, 38041 Grenoble Cedex 9, France

[∥]Departament de Química, Universitat Autònoma de Barcelona, Cerdanyola del Vallès, E-08193 Barcelona, Spain

[⊥]CNRS, UPR 8641, Centre de Recherche Paul Pascal (CRPP), Equipe "Matériaux Moléculaires Magnétiques", 115 avenue du Dr. Albert Schweitzer, Pessac, F-33600, France

[#]Université de Bordeaux, UPR 8641, Pessac, F-33600, France

[¶]CNRS, Université de Bordeaux, ICMCB, 87 avenue du Dr. Albert Schweitzer, Pessac, F-33600, France

Supporting Information

ABSTRACT: A new pentanuclear bis(triple-helical) manganese complex has been isolated and characterized by X-ray diffraction in two oxidation states: $[\{Mn^{II}(\mu\text{-bpp})_3\}_2Mn^{II}_2Mn^{III}(\mu\text{-O})]^{3+}$ ($\mathbf{1}^{3+}$) and $[\{Mn^{II}(\mu\text{-bpp})_3\}_2Mn^{II}Mn^{III}_2(\mu\text{-O})]^{4+}$ ($\mathbf{1}^{4+}$). The structure consists of a central $\{Mn_3(\mu_3\text{-O})\}$ core of $Mn^{II}_2Mn^{III}$ ($\mathbf{1}^{3+}$) or $Mn^{II}Mn^{III}_2$ ions ($\mathbf{1}^{4+}$) which is connected to two apical Mn^{II} ions through six bpp^- ligands. Both cations have a triple-stranded helicate configuration, and a pair of enantiomers is present in each crystal. The redox properties of $\mathbf{1}^{3+}$ have been investigated in CH_3CN. A series of five distinct and reversible one-electron waves is observed in the −1.0 and +1.50 V potential range, assigned to the $Mn^{II}_4Mn^{III}/Mn^{II}_5$, $Mn^{II}_3Mn^{III}_2/Mn^{II}_4Mn^{III}$, $Mn^{II}_2Mn^{III}_3/Mn^{II}_3Mn^{III}_2$, $Mn^{II}Mn^{III}_4/Mn^{II}_2Mn^{III}_3$, and $Mn^{III}_5/Mn^{II}Mn^{III}_4$ redox couples. The two first oxidation processes leading to $Mn^{II}_3Mn^{III}_2$ ($\mathbf{1}^{4+}$) and $Mn^{II}_2Mn^{III}_3$ ($\mathbf{1}^{5+}$) are related to the oxidation of the Mn^{II} ions of the central core and the two higher oxidation waves, close in potential, are thus assigned to the oxidation of the two apical Mn^{II} ions. The $\mathbf{1}^{4+}$ and $\mathbf{1}^{5+}$ oxidized species and the reduced Mn_4^{II} ($\mathbf{1}^{2+}$) species are quantitatively generated by bulk electrolyses demonstrating the high stability of the pentanuclear structure in four oxidation states ($\mathbf{1}^{2+}$ to $\mathbf{1}^{5+}$). The spectroscopic characteristics (X-band electron paramagnetic resonance, EPR, and UV−visible) of these species are also described as well as the magnetic properties of $\mathbf{1}^{3+}$ and $\mathbf{1}^{4+}$ in solid state. The powder X- and Q-band EPR signature of $\mathbf{1}^{3+}$ corresponds to an $S = 5/2$ spin state characterized by a small zero-field splitting parameter ($|D| = 0.071$ cm^{-1}) attributed to the two apical Mn^{II} ions. At 40 K, the magnetic behavior is consistent for $\mathbf{1}^{3+}$ with two apical $S = 5/2$ $\{Mn^{II}(bpp)_3\}^-$ and one $S = 2$ noninteracting spins (11.75 cm^3 K mol^{-1}), and for $\mathbf{1}^{4+}$ with three $S = 5/2$ noninteracting spins (13.125 cm^3 K mol^{-1}) suggesting that the $\{Mn^{II}_2Mn^{III}(\mu_3\text{-O})\}^{5+}$ and $\{Mn^{II}Mn^{III}_2(\mu_3\text{-O})\}^{6+}$ cores behave at low temperature like $S = 2$ and $S = 5/2$ spin centers, respectively. The thermal behavior below 40 K highlights the presence of intracomplex magnetic interactions between the two apical spins and the central core, which is antiferromagnetic for $\mathbf{1}^{3+}$ leading to an $S_T = 3$ and ferromagnetic for $\mathbf{1}^{4+}$ giving thus an $S_T = 15/2$ ground state.

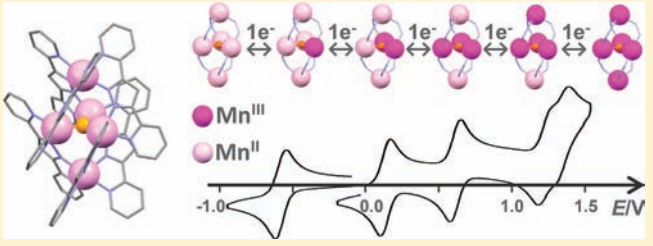

INTRODUCTION

Polynuclear manganese complexes have attracted much attention because of their relevance to the active centers of biological systems as the oxygen-evolving complex of photosystem II,[1−5] and also for the design of single-molecule magnets owing to their remarkable magnetic properties which result from the exchange interaction between paramagnetic centers.[6−12] Hundreds of such complexes have been isolated in the last decades in various nuclearity, core topology, and oxidation levels.[1,13−15] Their

Received: May 12, 2011
Published: August 03, 2011

Chart 1

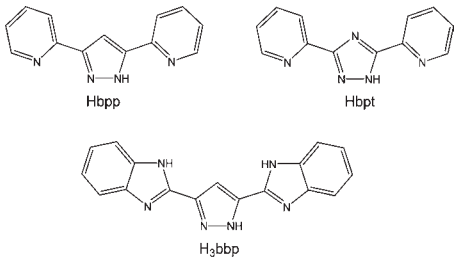

synthesis still relies on serendipitous self-assembly with appropriate ligands. Although carboxylates, Schiff base derivatives, alkoxides, and more recently oximes have been widely employed[16−25] as bridging ligands for the formation of these molecular manganese compounds, the use of pyrazole-based ligands is still limited.[26−31]

The 3,5-bis(pyridin-2-yl)-pyrazole ligand (Hbpp, Chart 1) is an attractive ligand of this family, which has led to the isolation of several dinuclear complexes with ruthenium[32−34] and various first row transition metal ions (Ni^{2+}, Cu^{2+}, Fe^{2+}, Co^{2+}, Zn^{2+}) either homo-[27,35−45] or heterobimetallic (Cr^{III}-$M^{II/III}$ with M = Fe^{2+}, Ln^{3+}, Mn^{2+}, and Ni^{2+})).[46−49] Very recently, some larger complexes having intriguing triple-helical structure have been also obtained, namely $[Fe^{II}{}_5(\mu_3\text{-O})(bpp)_6]^{2+}$ and $[M^{II}{}_5(\mu_3\text{−OH})(bpp)_6]^{3+}$ (M = Ni^{2+}, Zn^{2+}, or Cu^{2+}).[50−52] In these pentanuclear complexes, a central $\{M^{II}{}_3(\mu_3\text{-O})\}^{4+}$ or $\{M^{II}{}_3(\mu_3\text{-OH})\}^{5+}$ core is wrapped by two terminal $\{M^{II}(bpp)_3\}^-$ units, forming rare examples of helicates, in which metal cores define the helicate axis.[53−61] This $[M^{II}{}_5(\mu_3\text{-O})(L)_6]^{2+}$ helicate structure was also reported with two related L ligands, 3,5-bis-(benzimidazol-2-yl)pyrazole (H_3bbp, with M = Zn^{2+} and Cd^{2+})[57] and 3,5-bis(pyridin-2-yl)-1,2,4-triazole (Hbpt, for M = Fe^{2+}) (Chart 1).[62] The magnetic properties of the $[Cu^{II}{}_5(\mu_3\text{−OH})(bpp)_6]^{3+}$ and $[Fe^{II}{}_5(\mu_3\text{-O})(bpt)_6]^{2+}$ complexes have been deeply investigated. It has been shown that the helicate arrangement introduces peculiar magnetic properties such as spin-frustation in the case of the copper complex,[52] while for the iron complex the spin state of the two terminal iron(II) can be tuned by the nature of the counterion.[62]

Nevertheless, the use of the Hbpp ligand for the design of manganese compounds is restricted to the heterobimetallic dinuclear Cr^{III}-M^{II}.[49] In addition, the solution stability of the isolated $[M^{II}{}_5(\mu_3\text{-O})(L)_6]^{2+}$ and $[M^{II}{}_5(\mu_3\text{−OH})(bpp)_6]^{3+}$ compounds has been poorly investigated and limited to ESI-MS and ^1H NMR analyses[50,57] and their redox properties remain unexplored so far.

The aim of this work was to explore the formation of such polynuclear compounds with redox active manganese ions. In this line, we report here on the isolation of the first manganese pentanuclear bis(triple-helical) complex, namely $[Mn_5(\mu_3\text{-O})(bpp)_6]^{3+/4+}$, in which a $\{Mn_3(\mu_3\text{-O})\}^{5+/6+}$ core is wrapped by two terminal $\{Mn^{II}(bpp)_3\}^-$ units. An X-ray structure has been obtained in two oxidation states: $[\{Mn^{II}(\mu\text{-bpp})_3\}_2Mn^{II}{}_2Mn^{III}(\mu\text{-O})]^{3+}$ ($\mathbf{1}^{3+}$) and $[\{Mn^{II}(\mu\text{-bpp})_3\}_2Mn^{II}Mn^{III}{}_2(\mu\text{-O})]^{4+}$ ($\mathbf{1}^{4+}$). These manganese complexes are the first examples of such helicates that contain trivalent metal ion(s). Although many μ_3-O trinuclear complexes have been reported in the $Mn^{II}Mn^{III}{}_2$ and $Mn_3{}^{III}$ oxidation states,[1,12,19,21,24,31,63−71] to the best of our knowledge, $\mathbf{1}^{3+}$ contains the first example of an oxo-centered $\{Mn^{II}{}_2Mn^{III}(\mu_3\text{-O})\}^{5+}$ trinuclear unit. In addition, we report on the redox properties of this type of complex. Interestingly, the electrochemical study reveals that the manganese complex undergoes a series of reversible one-electron reduction and oxidation processes. Remarkably, the pentanuclear structure is perfectly stable in the following four oxidation states: $Mn^{II}{}_5$ ($\mathbf{1}^{2+}$), $Mn^{II}{}_4Mn^{III}$ ($\mathbf{1}^{3+}$), $Mn^{II}{}_3Mn^{III}{}_2$ ($\mathbf{1}^{4+}$), and $Mn^{II}{}_2Mn^{III}{}_3$ ($\mathbf{1}^{5+}$). As a consequence, this kind of polynuclear oxo-bridged manganese system might represent interesting potential catalysts for the oxidation of organic compounds, as recently demonstrated by Christou et al.[72] for the well-known Mn_{12} family, $[Mn_{12}O_{12}(OCR)_{16}(H_2O)_4]$ (R = Et, Ph, etc.), which also displays multiple one-electron reversible processes. Finally, the spectroscopic characteristics (X- and Q-band electron paramagnetic resonance, EPR, and UV−visible) and the magnetic properties of $\mathbf{1}^{3+}$ and $\mathbf{1}^{4+}$ in solid state have been investigated.

EXPERIMENTAL SECTION

Materials. The electrolytes tetra-*n*-butylammonium perchlorate, $[Bu_4N]ClO_4$, tetra-*n*-butylammonium tetrafluoroborate, $[Bu_4N]BF_4$, and acetonitrile (CH_3CN, Rathburn, HPLC grade) were used as received and stored under an argon atmosphere in a glovebox. The tetra-*n*-butylammonium hydroxide ($[Bu_4N]OH$, 40% in water, Fluka) and the ligand 3,5-bis(pyridin-2-yl)-pyrazole (Hbpp) (98%, TCI) were used as received.

Synthesis of $[\{Mn^{II}(\mu\text{-bpp})_3\}_2Mn_2{}^{II}Mn^{III}(\mu\text{-O})](ClO_4)_3$, $\mathbf{1}(ClO_4)_3$. *Method A.* A solution of $Mn(ClO_4)_2\cdot 6H_2O$ (120 mg, 0.33 mmol) in methanol (30 mL) was added to a stirred solution of Hbpp (106 mg, 0.47 mmol) and NaOH (19 mg, 0.47 mmol) in methanol (120 mL). The reaction mixture was refluxed for 2 h under air. To the resulting brown solution was added a saturated aqueous solution of $NaClO_4$. The precipitate formed was then filtered, redissolved in dichloromethane, and washed with water. The organic phase was then dried over Na_2SO_4 and the solvent was evaporated to dryness. The brown−black powder obtained was reprecipitated in CH_3CN/diethyl ether. Black single crystals of $\mathbf{1}(ClO_4)_3\cdot 2.5CH_3CN\cdot C_4H_{10}O\cdot 0.5H_2O$ were obtained by slow vapor diffusion of diethyl ether into an acetonitrile solution of the complex (yield: 80 mg, 61%). Elemental analysis calcd (%) for $C_{78}H_{54}Mn_5O_{13}N_{24}Cl_3\cdot 3.5H_2O$ (1979.52 g mol^{-1}): C 47.32; H, 3.10; N, 16.98. Found: C, 47.47; H, 2.96; N, 16.61. ESI-MS: *m/z* (%) 1187.1 (2) $[\{Mn^{II}(\mu\text{-bpp})_3\}_2Mn_2{}^{II}Mn^{III}(\mu\text{-O})(ClO_4)_2]^+$, 858.1 (25) $[\{Mn^{II}(\mu\text{-bpp})_3\}_2Mn_2{}^{II}Mn^{III}(\mu\text{-O})(ClO_4)]^{2+}$, 539.0 (100) $[\{Mn^{II}(\mu\text{-bpp})_3\}_2Mn_2{}^{II}Mn^{III}(\mu\text{-O})]^{3+}$.

Method B. A solution of $Mn(ClO_4)_2\cdot 6H_2O$ (135 mg, 0.37 mmol) in acetonitrile (10 mL) was added to a stirred solution of Hbpp (100 mg, 0.45 mmol) and Bu_4NOH (0.4 mL, 0.54 mmol) in acetonitrile (15 mL). The reaction mixture was refluxed for 4 h under air which led to the complete dissolution of the white precipitate formed initially. The resulting brown solution was then cooled to room temperature and filtered. Slow vapor diffusion of diethyl ether into this solution afforded black crystals of $\mathbf{1}(ClO_4)_3$. To obtain a pure sample of the complex, this recrystallization procedure was repeated several times (yield: 70 mg, 47%).

Caution! *Perchlorate salts of compounds containing organic ligands are potentially explosive. Although we have encountered no such problems, only small quantities of these compounds should be prepared and handled with care.*

Electrochemical Synthesis of $[\{Mn^{II}(\mu\text{-bpp})_3\}_2Mn^{II}Mn_2{}^{III}(\mu\text{-O})](ClO_4)_4$, $\mathbf{1}(ClO_4)_4$. A solution of $\mathbf{1}(ClO_4)_3$ (50 mg) in

dx.doi.org/10.1021/ic201009z |*Inorg. Chem.* 2011, 50, 8427–8436

acetonitrile (10 mL) containing 0.1 M of $[Bu_4N]ClO_4$ was oxidized at 0.35 V on a platinum plate under an argon atmosphere. Addition of diethyl ether to the solution after complete electrolysis (one electron exchanged per molecule of initial complex) led to the precipitation of $\mathbf{1}(ClO_4)_4$ which was filtered off and dried under air (yield: 36 mg, 70%). Elemental analysis calcd (%) for $C_{78}H_{54}Mn_5O_{17}N_{24}Cl_4 \cdot 3.5H_2O$ (2078.97 g mol^{-1}): C 45.06; H, 2.96; N, 16.17. Found: C, 45.08; H, 3.25; N, 16.22. Brown−black crystals of $\mathbf{1}(ClO_4)_4 \cdot 2CH_3CN \cdot 2C_4H_{10}O$ were obtained by slow vapor diffusion of diethyl ether into the electrolyzed solution.

X-ray Structure Determination. Data collection for $\mathbf{1}^{3+}$ was made on a Bruker-Nonius diffractometer equipped with an APPEX 2 4K CCD area detector, a FR591 rotating anode with Mo Kα radiation, Montel mirrors as monochromator, and a Kryoflex low temperature device (T = −173 °C). Full-sphere data collection was used with ω and φ scans. Programs used included data collection APEX-2,[73] data reduction Bruker Saint[74] V/.60A, and absorption correction SADABS.[75] For structure solution and refinement SHELXTL was used.[76] Diffraction data for $\mathbf{1}^{4+}$ were collected on a Bruker Smart Apex CCD diffractometer using graphite-monochromated Mo Kα radiation (λ = 0.71073 Å) from an X-ray tube. Programs were for data collection, Smart V. 5.631 (BrukerAXS 1997-02), data reduction, Saint+ Version 6.36A (Bruker AXS 2001), absorption correction, SADABS version 2.10 (Bruker AXS 2001), and structure solution and refinement, SHELXTL Version 6.14 (Bruker AXS 2000-2003).

Electrochemistry. All electrochemical measurements were made under an argon atmosphere in a dry-glovebox at room temperature. Cyclic voltammetry and controlled potential electrolysis experiments were performed by using an EG&G model 173 potentiostat/galvanostat equipped with a PAR model universal programmer and a PAR model 179 digital coulometer. A standard three-electrode electrochemical cell was used. Potentials were referred to an Ag/0.01 M $AgNO_3$ reference electrode in CH_3CN + 0.1 M $[Bu_4N]ClO_4$. Potentials referred to that system can be converted to the ferrocene/ferricinium couple by subtracting 87 mV, to SCE by adding 298 mV, or to NHE reference electrode by adding 0.548 V. The working electrodes were a platinum disk (5 mm in diameter) or a vitreous carbon disk (3 mm in diameter) polished with 2-μm diamond paste (Mecaprex Presi) for cyclic voltammetry (Ep_a, anodic peak potential; Ep_c, cathodic peak potential; $E_{1/2} = (Ep_a + Ep_c)/2$; $\Delta Ep = Ep_a - Ep_c$). Exhaustive electrolyses were carried out on reticulated vitreous carbon electrode 45 PPI (the electrosynthesis Co. Inc.; 1 cm^3) or on a platinum plate (5 cm^3). The auxiliary electrode was a Pt wire in CH_3CN + 0.1 M $[Bu_4N]ClO_4$.

Spectroscopy. X- and Q-band EPR spectra were recorded with a Bruker EMX. For the X-band, 100 K experiments, it was equipped with an ER-4192 ST Bruker cavity and an ER-4131 VT. For the 4.5 K experiments, an Oxford Instruments ESR-900 continuous-flow helium cryostat was used with an ER-4116 DM Bruker cavity for the X-band and an ER-5106 QTW Bruker cavity for the Q-band. For electrochemical experiments, electronic absorption spectra were recorded on a Varian Cary 50 or 100 absorption spectrophotometer. Initial and electrolyzed solutions were transferred to conventional quartz cells with 0.1 or 1 cm path length in the glovebox. The simulation of the powder EPR spectra of $\mathbf{1}^{3+}$ was performed with the SIM program written by Weihe and co-workers.[77] The parameters given in the text are issued from the best-simulated spectra obtained for each frequency.

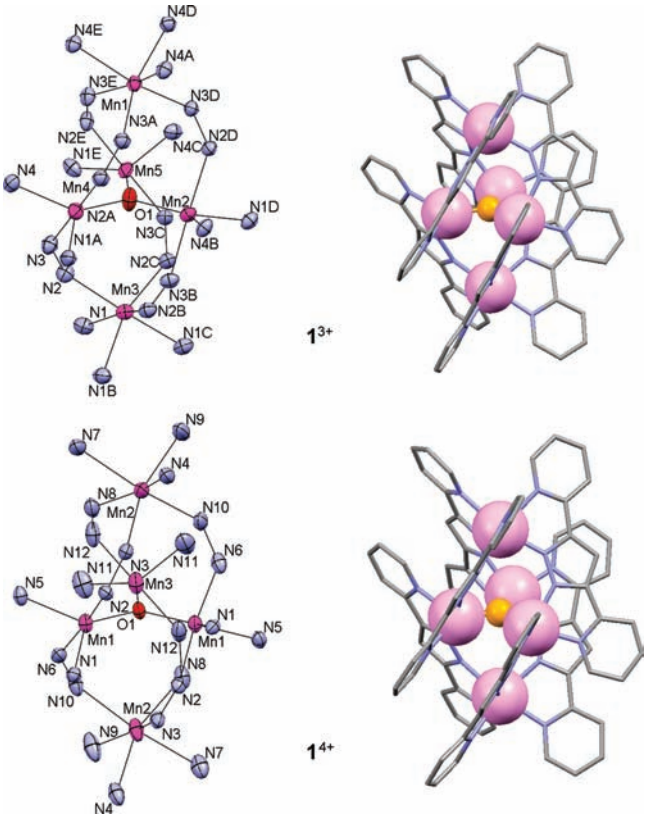

Figure 1. Structures of the $[\{Mn^{II}(\mu\text{-bpp})_3\}_2Mn^{II}_2Mn^{III}(\mu\text{-O})]^{3+}$ ($\mathbf{1}^{3+}$) and $[\{Mn^{II}(\mu\text{-bpp})_3\}_2Mn^{II}Mn^{III}_2(\mu\text{-O})]^{4+}$ ($\mathbf{1}^{4+}$) cations: left, ORTEP drawing (30% probability thermal ellipsoids), noncoordinated atoms of the bpp^- ligands omitted for clarity; right, ball-and-stick representation; Mn ions in pink and oxygen in orange.

Magnetic Susceptibility Measurements. The magnetic susceptibility measurements were obtained with the use of MPMS-XL Quantum Design SQUID magnetometer. This magnetometer works between 1.8 and 400 K for dc applied fields ranging from −7 to 7 T. Measurements were performed on polycrystalline samples of 18.73 and 13.00 mg for $\mathbf{1}^{3+}$ and $\mathbf{1}^{4+}$, respectively, introduced in a polyethylene bag (3 × 0.5 × 0.02 cm). The ac susceptibility measurements were measured with an oscillating ac field of 3 Oe with frequency between 1 to 1500 Hz. It is worth noting that no out-of-phase ac susceptibility signal has been detected above 1.8 K. The magnetic data were corrected for the sample holder (plastic bag) and the diamagnetic contribution.

RESULTS AND DISCUSSION

Synthesis of $\mathbf{1}(ClO_4)_3$ and $\mathbf{1}(ClO_4)_4$. $\mathbf{1}^{3+}$ has been synthesized in ∼50% yield from a methanolic or acetonitrile medium under aerobic conditions, by stirring a reaction mixture consisting of $Mn(ClO_4)_2 \cdot 6H_2O$ and bpp^- in a 5/6 molar ratio at reflux for few hours. The oxygen in air acts as an oxidant for the oxidation of one Mn^{II} ion of the complex into Mn^{III} leading to the isolation of the $Mn^{II}_4Mn^{III}$ oxidation state. This agrees with the negative potential value of $E_{1/2}$ = −0.58 V vs Ag^+/Ag for the $Mn^{II}_4Mn^{III}$/Mn^{II}_5 redox couple of the complex determined by electrochemistry (see Electrochemistry section). The $Mn^{II}_3Mn^{III}_2$ oxidation state ($\mathbf{1}^{4+}$) is obtained by electrochemical oxidation

dx.doi.org/10.1021/ic201009z |Inorg. Chem. 2011, 50, 8427–8436

of a solution of $\mathbf{1}^{3+}$ in acetonitrile (see Experimental Section). X-ray quality crystals of $\mathbf{1}^{3+}$ and $\mathbf{1}^{4+}$ were obtained by slow vapor diffusion of diethyl ether into solutions of the respective complex.

Crystal Structures of $1(ClO_4)_3\cdot 2.5CH_3CN\cdot C_4H_{10}O\cdot 0.5H_2O$ and $1(ClO_4)_4\cdot 2CH_3CN\cdot 2C_4H_{10}O$. Based on the charge of the cations, $\mathbf{1}^{3+}$ and $\mathbf{1}^{4+}$, and the presence of a μ_3-oxo bridge, the Mn oxidation states are given as $Mn^{II}_4Mn^{III}$ and $Mn^{II}_3Mn^{III}_2$, respectively. This mixed-valent description has been confirmed by a careful analysis of the X-ray structures, which evidenced the presence of Mn^{III} ion(s) in the central core (see below). The structures of $\mathbf{1}^{3+}$ and $\mathbf{1}^{4+}$ are shown in Figure 1 together with an ORTEP scheme of the central cores. Crystallographic data and selected bond distances and angles are reported in Tables 1, 2, and 3. The five Mn ions in $\mathbf{1}^{3+}$ and $\mathbf{1}^{4+}$ form a trigonal bipyramidal motif, in which the two Mn^{II} ions occupy the apical positions and the three Mn ions connected by a μ_3-O^{2-} ion are placed in the equatorial plane. The same topological motif was found in the single-molecule magnet $(NEt_4)_3[Mn_5O(salox)_3(N_3)_6Cl_2]$ (H_2salox = salicylaldoxime)[13,20,78] in which the three Mn^{III} ions are located in the equatorial position. The central $\{Mn_3(\mu_3\text{-}O)\}$ core of $Mn^{II}_2Mn^{III}$ ($\mathbf{1}^{3+}$) or $Mn^{II}Mn^{III}_2$ ions ($\mathbf{1}^{4+}$) is connected to the two apical Mn^{II} ions through six bpp^- ligands. Both cations have a triple-stranded helicate configuration and a pair of enantiomers is present in each crystal as previously observed in the other $[M^{II}_5(\mu_3\text{-}O)(L)_6]^{2+}$ and $[M^{II}_5(\mu_3\text{-}OH)(bpp)_6]^{3+}$ complexes.[50−52,57,62] In contrast to $\mathbf{1}^{3+}$, $\mathbf{1}^{4+}$ adopts a symmetric structure with a C_2 axis passing through the central Mn(3) and the μ_3-O ions that leads to the equivalence of the two remaining central manganese ions, Mn(1) and Mn(1)#, and also to the equivalence of the apical Mn(2) and Mn(2)#. In both compounds, the three Mn ions of the central core present a distorted N_4O trigonal bipyramid environment. The oxo bridging ligand is located in the equatorial plane together with two N-pyridine atoms of two bpp^- ligands while the axial positions are occupied by two N-pyrazole atoms of the latter bpp^- ligands. The trigonal indices for $\mathbf{1}^{3+}$ are of $\tau = 0.83$ (Mn(2)), 0.81 (Mn(4)), and 0.76 (Mn(5)), while for $\mathbf{1}^{4+}$ they are of $\tau = 0.65$ (Mn(1,1#)) and 0.82. (Mn(3)). The three Mn atoms form a nearly equilateral triangle with the oxygen in the center. For $\mathbf{1}^{3+}$, the central μ_3-O atom is slightly displaced from the Mn_3 triangular plane (0.033 Å), while for $\mathbf{1}^{4+}$, it lies on the C_2 axis and exactly in the plane of the Mn_3 triangle. All Mn···Mn distances in $\mathbf{1}^{3+}$ are significantly longer than those in $\mathbf{1}^{4+}$ ($Mn_{central}\cdots Mn_{central}$: av, 3.492 Å for $\mathbf{1}^{3+}$ and 3.279 Å for $\mathbf{1}^{4+}$; $Mn_{central}\cdots Mn_{terminal}$: av., 4.403 Å for $\mathbf{1}^{3+}$ and 4.281 Å for $\mathbf{1}^{4+}$).

The coordination geometry of the two apical Mn^{II} ions corresponds to a slightly distorted octahedron, consisting of six nitrogen atoms from three bridging bpp^- ligands. Each tetradentate bpp^- ligand bonds one apical and one equatorial Mn ion by one *N*-pyridine and one *N*-pyrazole. As usually observed in complexes with bpp^- ligand,[27,32−45,50−52,79,80] the Mn−*N*-pyridine distances are longer than the Mn−*N*-pyrazole ones.

Table 1. Crystal Data and Structure Refinement for $1(ClO_4)_3\cdot 2.5CH_3CN\cdot C_4H_{10}O\cdot 0.5H_2O$ and $1(ClO_4)_4\cdot 2CH_3CN\cdot 2C_4H_{10}O$

	$1(ClO_4)_3\cdot 2.5CH_3CN\cdot C_4H_{10}O\cdot 0.5H_2O$	$1(ClO_4)_4\cdot 2CH_3CN\cdot 2C_4H_{10}O$
chemical formula	$C_{87}H_{72.50}Cl_3Mn_5N_{26.50}O_{14.50}$	$C_{90}H_{80}Cl_4Mn_5N_{26}O_{19}$
formula weight	2102.26	2246.30
T, K	100	100
λ, Å	0.71073	0.71073
crystal system	monoclinic	monoclinic
space group	P2(1)/n	*C*2/*c*
a, Å	15.4109(7)	25.843(5)
b, Å	22.5910(10)	28.270(5)
c, Å	26.9272(11)	14.482(3)
α, deg	90.00	90.00
β, deg	101.9130(10)	93.709(3)
γ, deg	90.00	90.00
volume, Å^3	9172.7(7)	10559(3)
Z	4	4
density, mg m^{-3}	1.522	1.413
μ, mm^{-1}	0.836	0.759
F(000)	4288	4588
reflections collected	35236	12962
R_1[a]	0.0537	0.0848
wR_2[b]	0.1253	0.1927

[a] $R_1 = \Sigma||F_o| - |F_c||/\Sigma|F_o|$. [b] $wR_2 = [(\Sigma w(|F_o| - |F_c|)^2/\Sigma wF_o^2)]^{1/2}$.

Table 2. Selected Bond Lengths (Å) and Angles (°) for $1(ClO_4)_3\cdot 2.5CH_3CN\cdot C_4H_{10}O\cdot 0.5H_2O$

Mn(1)−N(3A)[a]	2.1878(19)	Mn(3)−N(2B)[a]	2.193(2)		
Mn(1)−N(3D)[a]	2.1971(19)	Mn(3)−N(2C)[a]	2.2170(19)		
Mn(1)−N(3E)[a]	2.216(2)	Mn(3)−N(2)[a]	2.210(2)		
Mn(1)−N(4E)[b]	2.305(2)	Mn(3)−N(1B)[b]	2.316(2)		
Mn(1)−N(4D)[b]	2.3078(19)	Mn(3)−N(1C)[b]	2.318(2)		
Mn(1)−N(4A)[b]	2.323(2)	Mn(3)−N(1)[b]	2.314(2)		
Mn(2)−O(1)	2.0442(17)	Mn(4)−O(1)	2.0156(17)	Mn(5)−O(1)	1.9894(17)
Mn(2)−N(2D)[a]	2.1547(18)	Mn(4)−N(2A)[a]	2.121(2)	Mn(5)−N(2E)[a]	2.077(2)
Mn(2)−N(3B)[a]	2.1448(19)	Mn(4)−N(3)[a]	2.122(2)	Mn(5)−N(3C)[a]	2.084(2)
Mn(2)−N(1D)[b]	2.202(2)	Mn(4)−N(4)[b]	2.181(2)	Mn(5)−N(1E)[b]	2.195(2)
Mn(2)−N(4B)[b]	2.223(2)	Mn(4)−N(1A)[b]	2.192(2)	Mn(5)−N(4C)[b]	2.191(2)
Mn(2)−Mn(5)	3.509(5)	Mn(2)−Mn(4)	3.491(5)	Mn(4)−Mn(5)	3.476(5)
Mn(1)−Mn(2)	4.455(5)	Mn(1)−Mn(4)	4.377(5)	Mn(1)−Mn(5)	4.410(5)
Mn(3)−Mn(2)	4.377(5)	Mn(3)−Mn(4)	4.433(5)	Mn(3)−Mn(5)	4.368(5)
Mn(4)−O(1)−Mn(2)	119.59(8)	Mn(5)−O(1)−Mn(2)	119.88(8)	Mn(5)−O(1)−Mn(4)	120.45(9)

[a] *N*-pyrazole. [b] *N*-pyridine.

dx.doi.org/10.1021/ic201009z |*Inorg. Chem.* 2011, 50, 8427–8436

Table 3. Selected Bond Lengths (Å) and Angles (deg) for $1(ClO_4)_4 \cdot 2CH_3CN \cdot 2C_4H_{10}O$

Mn(2)−N(8)[a]	2.179(5)				
Mn(2)−N(3)[a]	2.224(5)				
Mn(2)−N(10)[a]	2.229(5)				
Mn(2)−N(9)[b]	2.259(5)				
Mn(2)−N(4)[b]	2.268(6)				
Mn(2)- N(7)[b]	2.307(5)				
Mn(1)−O(1)[a]	1.870(3)	Mn(3)−O(1)	1.962(5)		
Mn(1)−N(2)[a]	1.932(4)	Mn(3)−N(12)[a]	2.024(5)		
Mn(1)−N(6)[a]	1.942(4)	Mn(3)−N(11)[b]	2.127(6)		
Mn(1)−N(5)[b]	2.090(4)				
Mn(1)−N(1)[b]	2.131(4)				
Mn(1)−Mn(1)#	3.238(2)	Mn(1)−Mn(3)	3.318(2)		
Mn(2)−Mn(1)	4.266(1)	Mn(2)−Mn(1)#	4.268(1)	Mn(2)−Mn(3)	4.294(1)
Mn(1)−O(1)−Mn(1) 120.0(3)		Mn(1)−O(1)−Mn(3) 120.02(13)			

As expected for its lower oxidation state, the position of the Mn^{II} ions in the complexes can be assigned on the basis of the longer Mn-ligand bond distances compared with the Mn^{III} ions. In both systems, the two apical Mn ions are thus readily assigned to Mn^{II} centers since their Mn−N bond distances are (i) longer than those of the central core, and (ii) poorly affected by the change of the oxidation state of the complex (in $\mathbf{1}^{3+}$: average 2.256 (0.062) Å for Mn(1) and 2.261 (0.060) Å for Mn(3); in $\mathbf{1}^{4+}$: average 2.244 (0.044) Å for Mn(2)). In addition, all Mn-ligand bond distances of the central core are significantly shorter in $\mathbf{1}^{4+}$ than in $\mathbf{1}^{3+}$, in accordance with an additional Mn^{III} ion in the central core of $\mathbf{1}^{4+}$.

Regarding the electron localization or delocalization in the central core, in $\mathbf{1}^{4+}$, the Mn(1,1#)−O(1) bond distances (1.870(3) Å) are notably shorter than the Mn(3)−O(1) bond distance (1.962(5) Å), and the Mn(1)···Mn(1)# bond distance (3.2384(16) Å) is shorter than the Mn(1,1#)···Mn(3) ones (3.319 Å). In fact, all bond distances to Mn(3) (average 2.053 (0.072) Å) are slightly longer than those for Mn(1,1#) (average, 1.993 (0.112) Å). By comparison with the structural characteristics of the previously reported valence-trapped $\{Mn^{II}Mn^{III}{}_2(\mu_3\text{-}O)\}^{6+}$ trinuclear complexes,[1,12,19,21,31,63−70] it can thus be concluded that the central core in $\mathbf{1}^{4+}$ is not fully localized with, nevertheless, the Mn(3) site that possesses a dominant +II oxidation state whereas Mn(1) and Mn(1#) have a dominant +III oxidation state.

Because, to our knowledge, the cation of $\mathbf{1}^{3+}$ contains the first example of an oxo-centered $\{Mn_2{}^{II}Mn^{III}(\mu_3\text{-}O)\}^{5+}$ trinuclear unit, the crystallographic characteristics of this core cannot be compared with literature data. One can however notice that the average of all bond distances of each Mn of the central core of $\mathbf{1}^{3+}$ (average 2.154 (0.069) Å (Mn(2)); average 2.126 (0.070) Å (Mn(4)) and average 2.107 (0.087) Å (Mn(5)) are too long for a localized Mn^{III} ion (expected value ≤2.0 Å). This indicates that the trinuclear center core of $\mathbf{1}^{3+}$ is probably a fully electron delocalized spin system.

Electrochemistry. The cyclic voltammogram of $\mathbf{1}^{3+}$ in CH_3CN (Figure 2A) displays one reversible reduction wave at $E_{1/2}$ = −0.58 V vs Ag^+/Ag (ΔEp = 70 mV) and four successive reversible oxidation waves at $E_{1/2}$ = +0.13 (ΔEp = 70 mV), +0.61 (ΔEp = 70 mV), +1.21 (ΔEp = 90 mV) and +1.33 V (ΔEp = 90 mV) at a scan rate of 100 mV·s^{-1}. Each of the five reversible redox processes corresponds to the exchange of one electron per molecule of complex as evidenced by rotating disk electrode experiments (not shown). These waves are assigned to the $Mn^{II}{}_4Mn^{III}/Mn^{II}{}_5$, $Mn^{II}{}_3Mn^{III}{}_2/Mn^{II}{}_4Mn^{III}$, $Mn^{II}{}_2Mn^{III}{}_3/Mn^{II}{}_3Mn^{III}{}_2$, $Mn^{II}Mn^{III}{}_4/Mn^{II}{}_2Mn^{III}{}_3$, and $Mn^{III}{}_5/Mn^{II}Mn^{III}{}_4$ redox couples, respectively. Bulk electrolysis experiments confirm that the reduction process and the two first oxidation processes correspond to the exchange of one electron. The two oxidized species, $Mn^{II}{}_3Mn^{III}{}_2$ ($\mathbf{1}^{4+}$) and $Mn^{II}{}_2Mn^{III}{}_3$ ($\mathbf{1}^{5+}$), are quantitatively generated (Figure 2B and C) by two successive electrolyses at E = +0.35 and E = +0.90 V of a solution of $\mathbf{1}^{3+}$. In contrast, the reduced $Mn_5{}^{II}$ species ($\mathbf{1}^{2+}$) has partially precipitated at the end of the electrolysis (E = −0.70 V) as an orange powder (Figure 2D). In all cases, back electrolyses restore quantitatively $\mathbf{1}^{3+}$, demonstrating the perfect reversibility of the different processes and the stability of the pentanuclear structure in four oxidation states, namely $Mn^{II}{}_5$ ($\mathbf{1}^{2+}$), $Mn^{II}{}_4Mn^{III}$ ($\mathbf{1}^{3+}$), $Mn^{II}{}_3Mn^{III}{}_2$ ($\mathbf{1}^{4+}$), and $Mn^{II}{}_2Mn^{III}{}_3$ ($\mathbf{1}^{5+}$). As verified by the X-ray diffraction analysis of crystals of $\mathbf{1}^{4+}$ (see above and Experimental Section), the two first oxidation processes located at +0.13 and +0.60 V leading to $\mathbf{1}^{4+}$ and $\mathbf{1}^{5+}$, are related to the oxidation of the Mn^{II} ions of the central core. The two last oxidation processes are thus related to the oxidation of the two apical Mn^{II} ions. The presence of two one-electron redox processes, closed in potential (+1.20 and +1.32 V), instead of a two-electron single wave, is in accordance with the presence of two identical electroactive centers in the molecule that can electronically communicate.[81,82] This is the case of the two apical Mn^{II} sites that can interact through the conjugation of the bridging bpp^- ligands and the central core. Attempts to electrogenerate the $Mn^{II}Mn^{III}{}_4$ ($\mathbf{1}^{6+}$) and $Mn^{III}{}_5$ ($\mathbf{1}^{7+}$) species have failed. Exhaustive electrolyses at E = +1.25 or +1.50 V involve a large excess of coulometry (5.5 electrons additional electrons per molecule of complex are exchanged) and lead to the full decomposition of the pentanuclear structure attested by the disappearance of the five initial waves on the resulting cyclic voltammogram. Moreover, several new irreversible redox processes are observed (two weakly intense, quasi-reversible, at $E_{1/2}$= +1.12 and 1.02 V, and two more intense, irreversible, at Ep_c = +0.38 and 0.0 V), which are not likely to correspond to a single species. Electrolyses performed at low temperature do not allow the stabilization of the $\mathbf{1}^{6+}$ and $\mathbf{1}^{7+}$ oxidation states.

The instability of $\mathbf{1}^{6+}$ and $\mathbf{1}^{7+}$ is probably due to the decoordination of some bpp^- ligands of the apical Mn^{III}. Indeed, Mn^{III} complexes containing solely nitrogen-based ligands are usually poorly stable and tend to form oxo-briged complexes by interaction with residual water in the solvent.[83−85] All electrogenerated solutions have also been analyzed by UV−visible (Figure 3)

dx.doi.org/10.1021/ic201009z |Inorg. Chem. 2011, 50, 8427–8436

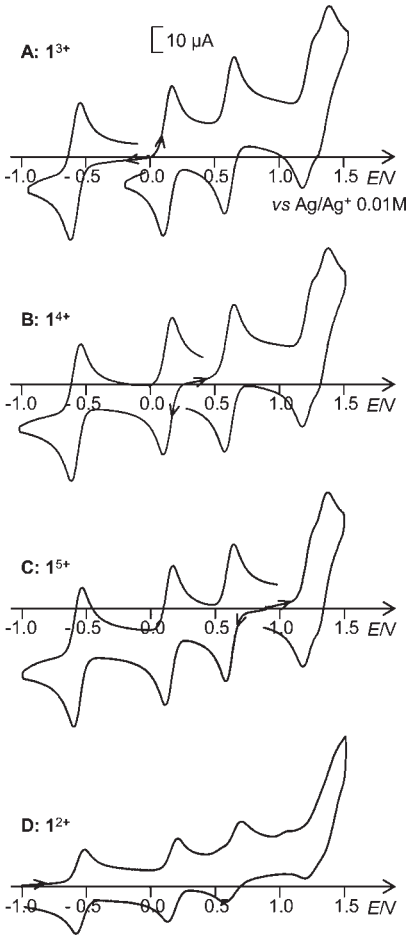

Figure 2. Cyclic voltammograms at a Pt electrode (diameter 5 mm) in CH_3CN, 0.1 M $[Bu_4N]ClO_4$ of (A) a 0.70 mM solution of $\mathbf{1}^{3+}$, (B) after exhaustive oxidation at +0.35 V of the (A) solution (formation of $\mathbf{1}^{4+}$), (C) after exhaustive oxidation at +0.90 V of the (B) solution (formation of $\mathbf{1}^{5+}$), (D) after exhaustive reduction at −0.70 V of the (A) solution (formation of $\mathbf{1}^{2+}$); scan rate of 100 mV·s^{-1}.

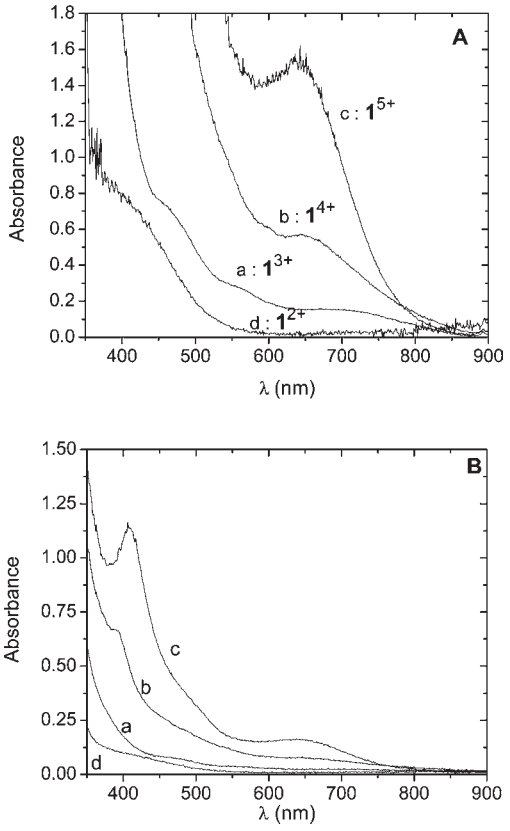

Figure 3. Visible absorption spectra changes during electrolyses of a 0.70 mM solution of $\mathbf{1}^{3+}$ in CH_3CN, 0.1 M $[Bu_4N]ClO_4$: (a) initial solution; (b) after oxidation at +0.35 V of the (a) solution (formation of $\mathbf{1}^{4+}$); (c) after oxidation at +0.90 V of the (b) solution (formation of $\mathbf{1}^{5+}$); (d) after reduction at −0.70 V of the (a) solution (formation of $\mathbf{1}^{2+}$); (A) l = 1 cm, (B) l = 1 mm.

and EPR spectroscopy (see below). The four stable oxidation states, from $\mathbf{1}^{2+}$ to $\mathbf{1}^{5+}$, have distinct UV−visible signatures. For each oxidation process, an increase of the absorbance in the visible region is observed consistent with the conversion of one Mn^{II} ion into Mn^{III}.[86,87]

The exceptional stability of the pentanuclear structure in four oxidation states ($\mathbf{1}^{2+}$ to $\mathbf{1}^{5+}$) is certainly due to its bis(triple-helical) structure that allows for maintaining the oxo-centered manganese trinuclear core at the $\{Mn_3^{II}(\mu_3\text{-O})\}^{4+}$, $\{Mn^{II}_2Mn^{III}(\mu_3\text{-O})\}^{5+}$, $\{Mn^{II}Mn^{III}_2(\mu_3\text{-O})\}^{6+}$, and $\{Mn_3^{III}(\mu_3\text{-O})\}^{7+}$ oxidation states. Indeed, although many oxo-centered trinuclear complexes have been reported in the $Mn^{II}Mn^{III}_2$ and Mn_3^{III} oxidation states, to our knowledge, there is no example of multinuclear Mn complexes with either a $\{Mn_3^{II}(\mu_3\text{-O})\}^{4+}$ or a $\{Mn^{II}_2Mn^{III}(\mu_3\text{-O})\}^{5+}$ unit as found in $\mathbf{1}^{2+}$ and in $\mathbf{1}^{3+}$. Divalent Mn ions solely are not prompted to stabilize O^{2-} ligands and the unique example of such trinuclear structure contains a μ_3−OH bridged core, i.e., $[(py)_5Mn_3^{II}(OAc)_3(\mu_3\text{−OH})(cat)]$.[88]

EPR Spectroscopy. The powder X- and Q-band EPR spectra of complex $\mathbf{1}^{3+}$ have been recorded between 30 and 100 K (Figure 4 displays the spectra obtained at 30 K). In this range of temperatures, the total intensity of the spectra decreases when increasing the temperature. This temperature behavior and the shape of the spectra are consistent with an S = 5/2 spin species.[85,89−91] As determined by magnetism (*vide infra*), the $\{Mn^{II}_2Mn^{III}(\mu_3\text{-O})\}^{5+}$ trinuclear unit corresponds to an S = 2 spin state below 40 K. However, no EPR signal, even in parallel mode, corresponding to this species is observed at 30 K, certainly due to the large zero-field splitting expected for Mn^{III} ions. Based on these data, we can conclude that the S = 5/2 signal can be assigned to the two equivalent apical Mn^{II} ions.

With the aim of confirming this hypothesis, simulations of the EPR spectra have been performed using a full-matrix diagonalization procedure of the spin Hamiltonian displayed in eq 1.

$$H = \mu_B\hat{H}\cdot[g]\cdot\hat{S} + D(\hat{S}_z^2 - 1/3\hat{S}^2) + E(\hat{S}_x^2 - \hat{S}_y^2) \qquad (1)$$

The first term represents the electronic Zeeman interaction with $\hat{H}$ being the magnetic field. The last two terms define the second-order (bilinear) *zfs* interaction with D and E representing the axial and rhombic parts, respectively. For neat powder EPR spectra, the ^{55}Mn hyperfine interaction is never resolved presumably because of the intermolecular dipole−dipole interactions together with the D-strain that contribute to the broadening of the line. Therefore, they have been omitted in eq 1. The good agreement obtained between the experimental and simulated spectra (Figure 4) confirms that these EPR spectra correspond to the signature of one Mn^{II} complex, implying that the two apical

dx.doi.org/10.1021/ic201009z |*Inorg. Chem.* 2011, 50, 8427–8436

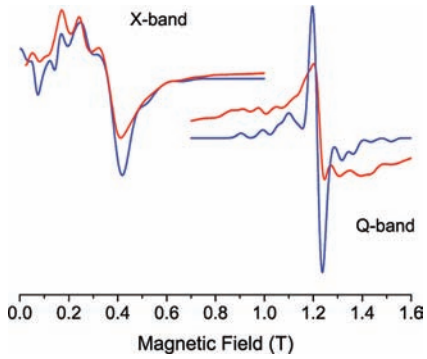

Figure 4. Experimental (red line) and simulated (blue line) powder X- and Q-band EPR spectra of $\mathbf{1}^{3+}$ recorded at 30 K. Parameters used for the simulation: at X-band $|D| = 0.073\ cm^{-1}$, $|E| = 0.008\ cm^{-1}$, $E/D = 0.110$, $g_x = g_y = g_z = 2.0$ and Q-band $|D| = 0.071\ cm^{-1}$, $|E| = 0.009\ cm^{-1}$, $E/D = 0.127$, $g_x = g_y = g_z = 2.0$.

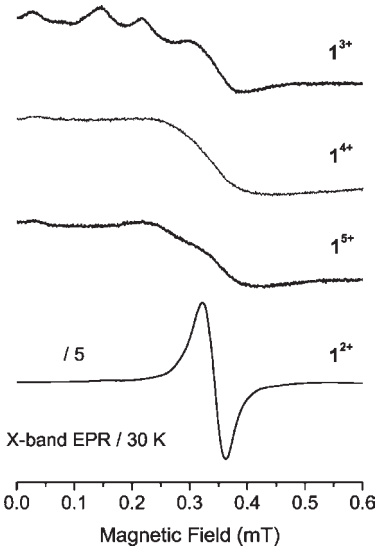

Figure 5. X-band EPR at 30 K of 0.70 mM solution of $\mathbf{1}^{3+}$ in CH_3CN, 0.1 M $[Bu_4N]ClO_4$ and of the electrogenerated solutions of $\mathbf{1}^{4+}$, $\mathbf{1}^{5+}$, and $\mathbf{1}^{2+}$.

Mn^{II} units are equivalent. In addition, the $|D|$ parameter of $0.071\ cm^{-1}$ (0.102 K), issued from the Q-band EPR spectrum for which the high field limit conditions are reached ($D \ll h\nu$), is consistent with an N6 environment, when compared with the literature ($0.010 < |D_{N6}| < 0.175\ cm^{-1}$).[91]

The X-band EPR spectra in solution of $\mathbf{1}^{3+}$ and of the electrogenerated solutions of $\mathbf{1}^{4+}$, $\mathbf{1}^{5+}$, and $\mathbf{1}^{2+}$ have been recorded between 5 and 50 K (Figure 5 shows the EPR spectra at 30 K). In this range of temperatures, the global intensity of the spectra decreases with increasing temperatures for all the species, while the relative intensity and the broadening of the lines are not affected by the temperature. The EPR spectrum of $\mathbf{1}^{3+}$ in solution is comparable to that recorded on powder (Figure 4), demonstrating that the structure of the complex is retained in solution, with the two magnetic-independent apical Mn(II) ions. The shape of the EPR spectrum of $\mathbf{1}^{4+}$ drastically changes compared to $\mathbf{1}^{3+}$ with a notable broadening of the resonance lines. This attests that in $\mathbf{1}^{4+}$, the two apical $\{Mn^{II}(bpp)_3\}^{-}$ units are in magnetic interaction between each other, and/or more likely with the central core.

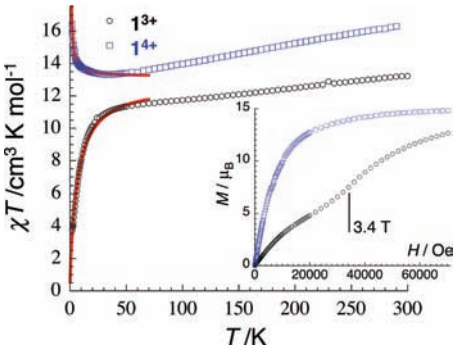

Figure 6. Temperature dependence of the χT products (where $\chi = M/H$ per $[Mn_5]$ complex) measured at 0.1 T and inset: field dependence of the magnetization at 1.8 K for compound $\mathbf{1}^{3+}$ (black open dots) and $\mathbf{1}^{4+}$ (blue open squares). The solid red lines are the best fits to the Heisenberg model described in the text.

The EPR spectrum of $\mathbf{1}^{5+}$ is comparable to that $\mathbf{1}^{4+}$. Concerning $\mathbf{1}^{2+}$, the EPR spectrum is significantly modified with respect to $\mathbf{1}^{3+}$. A unique signal centered at $g = 2$ is observed that can tentatively be attributed to the sum of the spectra corresponding to five Mn^{II} ions. After the full oxidation of the solution of the complex at $E = 1.50$ V, only a weak six-line EPR signal is observed (not shown), characteristic of $Mn^{II}(CH_3CN)_6^{2+}$,[92,93] that is formed in a very small amount.

Magnetic Properties of $\mathbf{1}^{3+}$ and $\mathbf{1}^{4+}$. The magnetic properties of $\mathbf{1}^{3+}$ and $\mathbf{1}^{4+}$ have been studied on powder samples of $\mathbf{1}(ClO_4)_3 \cdot 2.5CH_3CN \cdot C_4H_{10}O \cdot 0.5H_2O$ and $\mathbf{1}(ClO_4)_4 \cdot 2CH_3CN \cdot 2C_4H_{10}O$. Between 300 and 40 K, the χT products decrease very slowly, from 13.3 and 16.3 $cm^3\ K\ mol^{-1}$ for $\mathbf{1}^{3+}$ and $\mathbf{1}^{4+}$ to a pseudoplateau around 40 K at 11.2 and 13.4 $cm^3\ K\ mol^{-1}$, respectively (Figure 6). Below 40 K, the two compounds show different magnetic behaviors: the χT product is again decreasing for $\mathbf{1}^{3+}$ but in a more abrupt fashion to reach the value of 3.7 $cm^3\ K\ mol^{-1}$ at 1.8 K, while it is increasing for $\mathbf{1}^{4+}$ to reach the value of 16.5 $cm^3\ K\ mol^{-1}$ at 1.8 K. At room temperature, the χT products are low in comparison to the values of 20.5 and 19.125 $cm^3\ K\ mol^{-1}$ expected for high-spin Mn^{II} ($S = {}^5/_2$, $g \approx 2$) and high-spin Mn^{III} ($S = 2$, $g \approx 2$) centers in 4:1 and 3:2 ratio in $\mathbf{1}^{3+}$ and $\mathbf{1}^{4+}$, respectively. On the other hand, both χT values measured at 40 K are in very good agreement with two apical $S = 5/2$ $\{Mn^{II}(bpp)_3\}^{-}$ ($C = 4.375\ cm^3\ K\ mol^{-1}$ with $g = 2$) and one $S = 2$ ($C = 3\ cm^3\ K\ mol^{-1}$ with $g = 2$) noninteracting spins ($11.75\ cm^3\ K\ mol^{-1}$) for $\mathbf{1}^{3+}$ and with three $S = 5/2$ noninteracting spins ($13.125\ cm^3\ K\ mol^{-1}$) for $\mathbf{1}^{4+}$. This result suggests that the $\{Mn^{II}{}_2Mn^{III}(\mu_3\text{-}O)\}^{5+}$ and $\{Mn^{II}Mn^{III}{}_2(\mu_3\text{-}O)\}^{6+}$ cores behave at low temperature like $S = 2$ and $S = 5/2$ spin centers, respectively.

To explain the trinuclear core magnetic behavior above 40 K, two approaches can be envisioned. The first hypothesis is to consider electrons and thus spins localized on each manganese site. In this case, the magnetic data above 40 K should fit with simple Heisenberg triangular models with an $S_i = 5/2$; $5/2$; 2 set of spins for $\mathbf{1}^{3+}$ or an $S_i = 5/2$; 2; 2 set of spins for $\mathbf{1}^{4+}$ and intracore antiferromagnetic interactions. Unfortunately, we have been unable to reproduce, even qualitatively, the temperature dependence of the susceptibility above 40 K using this approach. Therefore the observed thermal behavior has to be explained in the frame of a delocalized model in which each trinuclear core is considered as an "entity" with a given spin. This approach is

dx.doi.org/10.1021/ic201009z |Inorg. Chem. 2011, 50, 8427–8436

indeed in good agreement with the structural analysis described above. As mentioned previously, the magnetic data suggest that the ground state of the $\{Mn^{II}_2Mn^{III}(\mu_3\text{-}O)\}^{5+}$ and $\{Mn^{II}Mn^{III}_2(\mu_3\text{-}O)\}^{6+}$ cores are, respectively, $S = 2$ and $S = 5/2$. Then the increase of the χT product above 40 K is simply the signature of the thermal population of the low-lying excited spin states of the trinuclear core as it is observed for spin-crossover complexes.

Below 40 K, the trinuclear core of the complex can be considered as a single localized spin ($S = 2$ and $S = 5/2$ for $\mathbf{1}^{3+}$ and $\mathbf{1}^{4+}$, respectively) and therefore taking into account the two apical $S = 5/2$ $\{Mn^{II}(bpp)_3\}^-$ motifs, the magnetic properties of the complexes can be modeled using the following Heisenberg spin Hamiltonian:

$$H = -2JS_C(S_{Mn1} + S_{Mn2}) \quad (2)$$

with S_C and S_{Mni} being the spins of the central trinuclear core and the apical Mn(II) metal ions, respectively. For $\mathbf{1}^{4+}$, the increase of the χT product below 40 K is clearly indicative of intracomplex ferromagnetic interactions between $S = 5/2$ spins. This magnetic exchange is well estimated at +0.05(1) K ($g = 2.0(1)$) from the fit of the experimental data to the analytical theoretical susceptibility (see Supporting Information) in the low field approximation (red line on the blue squares, Figure 6) deduced from eq 2 and the application of the van Vleck equation.[94,95] The field dependence of the magnetization for $\mathbf{1}^{4+}$ at 1.8 K, shown in the inset of Figure 6, confirms the presence of ferromagnetic interactions with a rapid increase of the magnetization at low field. Indeed, antiferromagnetic interactions would lead to an "S" shape curve. It is worth further mentioning that the magnetization reaches 14.9 μ_B in very good agreement with the presence of three $S = 5/2$ spins (note that the M vs H data at 1.8 K are well fitted to a sum of three $S = 5/2$ Brillouin functions with $g = 2.0$ in accord with very weak interactions) and thus an $S_T = 15/2$ ground state for this complex induced by the intracomplex ferromagnetic couplings.

The analysis of the magnetic behavior for $\mathbf{1}^{3+}$ below 40 K is not so straightforward. The decrease of the χT product below 40 K highlights the presence of intracomplex antiferromagnetic interactions between apical $S = 5/2$ spins and the central trinuclear core considered as an effective $S = 2$ spin at these temperatures. The presence of this antiferromagnetic interaction is further supported by the M vs H plot at 1.8 K (inset of Figure 6) that displays a clear inflection point around 3.4 T. Considering that this field, H^*, corresponds to the energy necessary to overcome the intracomplex antiferromagnetic interactions (i.e., to have all the spins aligned in the applied dc field), the following relation is obtained: $8JS_{Mni}S_C = -2g\mu_B HS_C$ from eq 2 and thus the equality between the exchange and the Zeeman energies. Therefore the intracomplex antiferromagnetic interaction between apical $S = 5/2$ spins and the central trinuclear spin is estimated at −0.45 K (with $g = 2$). At high field, the magnetization increases without clear saturation and reaches 12.7 μ_B at 7 T (inset Figure 6) in agreement with the field alignment of two $S = 5/2$ and one $S = 2$ spins (expected saturation value at 14 μ_B). In parallel, the χT vs T data (Figure 6) below 40 K have been modeled using the same analytical approach (eq 2) as for $\mathbf{1}^{3+}$ but this time, the experimental data could be reproduced only introducing additional intercomplex magnetic interactions (in the frame of the mean field approximation).[96] The comparison between the crystal packing of $\mathbf{1}^{3+}$ and $\mathbf{1}^{4+}$ reveals that the Mn...Mn distances between the closest ions are significantly longer in $\mathbf{1}^{4+}$, consistent with stronger intermolecular interactions in $\mathbf{1}^{3+}$. The best fit shown in solid red line in Figure 6 (on the open black dots) corresponds to $J/k_B = -0.40(5)$ K, $zJ'/k_B = -0.19(3)$ K and $g = 2.0(1)$. It is worth noting that the intracomplex interactions deduced from the M vs H and the χT vs T data are perfectly consistent around −0.4 K and thus induce an $S_T = 3$ ground state for $\mathbf{1}^{3+}$ but that the intercomplex interactions, zJ', are certainly overestimated by this modeling approach as their value also contains phenomenologically the effects of the magnetic anisotropy brought by the Mn^{III} metal ion. Attempts to simulate numerically the experimental data (M vs H and χT vs T) for $\mathbf{1}^{3+}$ including both effects failed and lead to multiple solutions and thus overparametrization of the simulation.

Finally, the magnetic measurements demonstrate that the controlled oxidation of $\mathbf{1}^{3+}$ in $\mathbf{1}^{4+}$ induces a change of effective spin state of the delocalized $\{Mn_3(\mu_3\text{-}O)\}$ core from $S = 2$ to $S = 5/2$ and convert an $S_T = 3$ $[Mn_5]$ complex into an $S_T = 15/2$ system.

CONCLUSIONS

We have isolated and structurally characterized a new pentanuclear manganese complex, namely $[\{Mn^{II}(\mu\text{-bpp})_3\}_2Mn^{II}_2Mn^{III}(\mu\text{-O})]^{3+}$ ($\mathbf{1}^{3+}$), by reacting Mn^{2+} ions and the rigid tetradentate bis(pyridyl)-pyrazolate ligand as well as its electrogenerated one-electron oxidized form, $[\{Mn^{II}(\mu\text{-bpp})_3\}_2Mn^{II}Mn^{III}_2(\mu\text{-O})]^{4+}$ ($\mathbf{1}^{4+}$). These complexes join the small family of bis(triple-helical) pentanuclear complexes featuring a triangular oxo-centered $\{M^{II}_3(\mu_3\text{-O})\}^{4+}$ (M = Fe^{2+} or Cd^{2+}) or $\{M^{II}_3(\mu_3\text{−}OH)\}^{5+}$ (M = Ni^{2+}, Zn^{2+} or Cu^{2+}) connected to two apical $\{M^{II}(L)_3\}^-$ units (L = bpp^- or bpt^-). In contrast to all these previously reported helicate compounds, which contain only divalent metallic ions, the aerobic condition used for the synthesis of $\mathbf{1}^{3+}$ has led to its isolation in a mixed divalent and trivalent oxidation states.

Furthermore, $\mathbf{1}^{3+}$ exhibits very rich redox behavior with five distinct and reversible one-electron processes located between −1.0 and +1.5 V. In addition, bulk electrolyses have evidenced the exceptional stability of the complex in four oxidation states. Indeed, the oxidation states of the oxo-centered trinuclear core can switch among $\{Mn_3^{II}(\mu_3\text{-}O)\}^{4+}$, $\{Mn^{II}_2Mn^{III}(\mu_3\text{-}O)\}^{5+}$, $\{Mn^{II}Mn^{III}_2(\mu_3\text{-}O)\}^{6+}$, and $\{Mn_3^{III}(\mu_3\text{-}O)\}^{7+}$, while the two Mn apical ions remain at the +II oxidation state. The peculiar bis(triple-helical) structure certainly allows for the unusual stability of the $\{Mn_3^{II}(\mu_3\text{-}O)\}^{4+}$ and $\{Mn^{II}_2Mn^{III}(\mu_3\text{-}O)\}^{5+}$ oxidation levels since, to our knowledge, there is no example of trinuclear or larger multinuclear Mn complexes presenting such motif at these low oxidation states.

From magnetic measurements, it appears that the one-electron oxidation of $\mathbf{1}^{3+}$ to $\mathbf{1}^{4+}$ induces a change of the nature of the magnetic intracomplex interaction between the two apical Mn^{II} and the $\{Mn_3(\mu_3\text{-}O)\}^{5+/6+}$ central core from antiferromagnetic to ferromagnetic coupling, converting an $S_T = 3$ into an $S_T = 15/2$ spin ground state system.

Finally, our study provides the first report on the exploration of the redox properties of such complexes and evidenced how rich they are with the unexpected and excellent stability in solution of the pentanuclear manganese entity in four oxidation states. This particular compound is thus capable to exchange four electrons, and is a good promising candidate suitable to catalyze oxidation reactions. Further work is in progress in our laboratories to test its performance in such reactions.

dx.doi.org/10.1021/ic201009z |Inorg. Chem. 2011, 50, 8427–8436

■ ASSOCIATED CONTENT

Supporting Information. Crystallographic data for $\mathbf{1}^{3+}$ and $\mathbf{1}^{4+}$ in CIF format and equations used for magnetic susceptibility analysis. This material is available free of charge via the Internet at http://pubs.acs.org. CCDC 818591 and 818592 contain the supplementary crystallographic data for this paper. These data can be obtained free of charge via www.ccdc.cam.ac.uk/data_request/cif, or by emailing data_request@ccdc.cam.ac.uk, or by contacting The Cambridge Crystallographic Data Centre, 12, Union Road, Cambridge CB2 1EZ, UK; fax: +44 1223 336033.

■ AUTHOR INFORMATION

Corresponding Author

*E-mail: allobet@iciq.es (A.L.), montse.rodriguez@udg.edu (M.R.), marisa.romero@udg.es (I.R.), marie-noelle.collomb@ujf-grenoble.fr (M.-N.C.).

■ ACKNOWLEDGMENT

T.S. thanks the Département de Chimie Moléculaire for his PhD grant. J.R., C.S., M.R., and I.R. thank MICINN of Spain through project CTQ2010-21532-C02-01 for financial support. J.R. also thanks UdG for the allocation of a BR predoctoral grant. R.C. and C.M thank the University of Bordeaux, the ANR (NT09_469563, AC-MAGnets project), the Région Aquitaine, the GIS Advanced Materials in Aquitaine (COMET Project), and the CNRS for financial support. Thanks are also given to SOLAR-H2 (EU 212508) and the MICINN (Consolider Ingenio 2010 (CSD2006-0003), CTQ2010-67918).

■ REFERENCES

(1) Mukhopadhyay, S.; Mandal, S. K.; Bhaduri, S.; Armstrong, W. H. *Chem. Rev.* **2004**, *104*, 3981–4026.
(2) Weatherburn, D. C.; Mandal, S.; Mukhopadhyay, S.; Bahduri, S.; Lindoy, L. F. Manganese. In *Comprehensive Coordination Chemistry II*; McCleverty, J. A., Meyer, T. J., Eds.; Elsevier Pergamon: Oxford, 2004; Vol. 5, p 1.
(3) Wu, A. J.; Penner-Hahn, J. E.; Pecoraro, V. L. *Chem. Rev.* **2004**, *104*, 903–938.
(4) Mullins, C. S.; Pecoraro, V. L. *Coord. Chem. Rev.* **2008**, *252*, 416–443.
(5) Collomb, M.-N.; Deronzier, A. *Eur. J. Inorg. Chem.* **2009**, 2025–2046.
(6) Gatteschi, D.; Sessoli, R. *Angew. Chem., Int. Ed.* **2003**, *42*, 268–297.
(7) Bagai, R.; Christou, G. *Chem. Soc. Rev.* **2009**, *38*, 1011–1026.
(8) Roubeau, O.; Clérac, R. *Eur. J. Inorg. Chem.* **2008**, 4325–4342.
(9) Hill, S.; Datta, S.; Liu, J.; Inglis, R.; Milios, C. J.; Feng, P. L.; Henderson, J. J.; del Barco, E.; Brechin, E. K.; Hendrickson, D. N. *Dalton Trans.* **2010**, *39*, 4693–4707.
(10) Milios, C. J.; Vinslava, A.; Wernsdorfer, W.; Moggach, S.; Parsons, S.; Perlepes, S. P.; Christou, G.; Brechin, E. K. *J. Am. Chem. Soc.* **2007**, *129*, 2754–2755.
(11) Milios, C. J.; Inglis, R.; Vinslava, A.; Bagai, R.; Wernsdorfer, W.; Parsons, S.; Perlepes, S. P.; Christou, G.; Brechin, E. K. *J. Am. Chem. Soc.* **2007**, *129*, 12505–12511.
(12) Stamatatos, T. C.; Foguet-Albiol, D.; Lee, S. C.; Stoumpos, C. C.; Raptopoulou, C. P.; Terzis, A.; Wernsdorfer, W.; Hill, S. O.; Perlepes, S. P.; Christou, G. *J. Am. Chem. Soc.* **2007**, *129*, 9484–9499.
(13) Kostakis, G. E.; Ako, A. M.; Powell, A. K. *Chem. Soc. Rev.* **2010**, *39*, 2238–2271.
(14) Chen, H. Y.; Collomb, M. N.; Duboc, C.; Blondin, G.; Riviere, E.; Faller, J. W.; Crabtree, R. H.; Brudvig, G. W. *Inorg. Chem.* **2005**, *44*, 9567–9573.
(15) Baffert, C.; Orio, M.; Pantazis, D. A.; Duboc, C.; Blackman, A. G.; Blondin, G.; Neese, F.; Deronzier, A.; Collomb, M. N. *Inorg. Chem.* **2009**, *48*, 10281–10288.
(16) Nayak, S.; Evangelisti, M.; Powell, A. K.; Reedijk, J. *Chem.—Eur. J.* **2010**, *16*, 12865–12872.
(17) Milios, C. J.; Stamatatos, T. C.; Perlepes, S. P. *Polyhedron* **2006**, *25*, 134–194.
(18) Afrati, T.; Dendrinou-Samara, C.; Raptopoulou, C. R.; Terzis, A.; Tangoulis, V.; Kessissoglou, D. P. *Angew. Chem., Int. Ed.* **2002**, *41*, 2148–2150.
(19) Sreerama, S. G.; Pal, S. *Inorg. Chem.* **2002**, *41*, 4843–4845.
(20) Yang, C. I.; Wernsdorfer, W.; Lee, G. H.; Tsai, H. L. *J. Am. Chem. Soc.* **2007**, *129*, 456–457.
(21) Yang, C. I.; Wernsdorfer, W.; Cheng, K. H.; Nakano, M.; Lee, G. H.; Tsai, H. L. *Inorg. Chem.* **2008**, *47*, 10184–10186.
(22) Pathmalingam, T.; Gorelsky, S. I.; Burchell, T. J.; Bedard, A. C.; Beauchemin, A. M.; Clérac, R.; Murugesu, M. *Chem. Commun.* **2008**, 2782–2784.
(23) Inglis, R.; Jones, L. F.; Milios, C. J.; Datta, S.; Collins, A.; Parsons, S.; Wernsdorfer, W.; Hill, S.; Perlepes, S. P.; Piligkos, S.; Brechin, E. K. *Dalton Trans.* **2009**, 3403–3412.
(24) Manolopoulou, E.; Stoumpos, C. C.; Siczek, M.; Lis, T.; Brechin, E. K.; Milios, C. J. *Eur. J. Inorg. Chem.* **2010**, 483–489.
(25) Inglis, R.; Stoumpos, C. C.; Prescimone, A.; Siczek, M.; Lis, T.; Wernsdorfer, W.; Brechin, E. K.; Milios, C. J. *Dalton Trans.* **2010**, *39*, 4777–4785.
(26) van der Vlugt, J. I.; Demeshko, S.; Dechert, S.; Meyer, F. *Inorg. Chem.* **2008**, *47*, 1576–1585.
(27) Klingele, J.; Dechert, S.; Meyer, F. *Coord. Chem. Rev.* **2009**, *253*, 2698–2741.
(28) Penkova, L.; Demeshko, S.; Pavlenko, V. A.; Dechert, S.; Meyer, F.; Fritsky, I. O. *Inorg. Chim. Acta* **2010**, *363*, 3036–3040.
(29) Viciano-Chumillas, M.; Tanase, S.; de Jongh, L. J.; Reedijk, J. *Eur. J. Inorg. Chem.* **2010**, 3403–3418.
(30) Viciano-Chumillas, M.; de Ruiter, G.; Tanase, S.; Smits, J. M. M.; de Gelder, R.; Mutikainen, I.; Turpeinen, U.; de Jongh, L. J.; Reedijk, J. *Dalton Trans.* **2010**, *39*, 4991–4998.
(31) Viciano-Chumillas, M.; Tanase, S.; Roubeau, O.; Teat, S. J.; de Jongh, L. J.; Reedijk, J. *Eur. J. Inorg. Chem.* **2010**, 947–951.
(32) Sens, C.; Romero, I.; Rodriguez, M.; Llobet, A.; Parella, T.; Benet-Buchholz, J. *J. Am. Chem. Soc.* **2004**, *126*, 7798–7799.
(33) Bozoglian, F.; Romain, S.; Ertem, M. Z.; Todorova, T. K.; Sens, C.; Mola, J.; Rodriguez, M.; Romero, I.; Benet-Buchholz, J.; Fontrodona, X.; Cramer, C. J.; Gagliardi, L.; Llobet, A. *J. Am. Chem. Soc.* **2009**, *131*, 15176–15187.
(34) Planas, N.; Christian, G. J.; Mas-Marza, E.; Sala, X.; Fontrodona, X.; Maseras, F.; Llobet, A. *Chem.—Eur. J.* **2010**, *16*, 7965–7968.
(35) Casabo, J.; Pons, J.; Siddiqi, K. S.; Teixidor, F.; Molins, E.; Miravitlles, C. *J. Chem. Soc., Dalton Trans.* **1989**, 1401–1403.
(36) Pons, J.; Lopez, X.; Benet, E.; Casabo, J.; Teixidor, F.; Sanchez, F. J. *Polyhedron* **1990**, *9*, 2839–2845.
(37) Pons, J.; Lopez, X.; Casabo, J.; Teixidor, F.; Caubet, A.; Rius, J.; Miravitlles, C. *Inorg. Chim. Acta* **1992**, *195*, 61–66.
(38) Pons, J.; Sanchez, F. J.; Labarta, A.; Casabo, J.; Teixidor, F.; Caubet, A. *Inorg. Chim. Acta* **1993**, *208*, 167–171.
(39) Munakata, M.; Wu, L. P.; Yamamoto, M.; KurodaSowa, T.; Maekawa, M.; Kawata, S.; Kitagawa, S. *J. Chem. Soc., Dalton Trans.* **1995**, 4099–4106.
(40) Nakano, K.; Suemura, N.; Kawata, S.; Fuyuhiro, A.; Yagi, T.; Nasu, S.; Morimoto, S.; Kaizaki, S. *Dalton Trans.* **2004**, 982–988.
(41) Nakano, K.; Kawata, S.; Yoneda, K.; Fuyuhiro, A.; Yagi, T.; Nasu, S.; Morimoto, S.; Kaizaki, S. *Chem. Commun.* **2004**, 2892–2893.
(42) Yoneda, K.; Nakano, K.; Fujioka, J.; Yamada, K.; Suzuki, T.; Fuyuhiro, A.; Kawata, S.; Kaizaki, S. *Polyhedron* **2005**, *24*, 2437–2442.
(43) Du, M.; Chen, S. T.; Guo, Y. M.; Bu, X. H.; Ribas, J. *J. Mol. Struct.* **2005**, *737*, 17–21.
(44) Yoneda, K.; Adachi, K.; Hayami, S.; Maeda, Y.; Katada, M.; Fuyuhiro, A.; Kawata, S.; Kaizaki, S. *Chem. Commun.* **2006**, 45–47.

(45) Ishikawa, R.; Fuyuhiro, A.; Hayami, S.; Inoue, K.; Kawata, S. *J. Mol. Struct.* **2008**, *892*, 220–224.
(46) Ni-iya, K.; Fuyuhiro, A.; Yagi, T.; Nasu, S.; Kuzushita, K.; Morimoto, S.; Kaizaki, S. *Bull. Chem. Soc. Jpn.* **2001**, *74*, 1891–1897.
(47) Kawahata, R.; Tsukuda, T.; Yagi, T.; Subhan, A.; Nakata, H.; Fuyuhiro, A.; Kaizaki, S. *Chem. Lett.* **2003**, *32*, 1084–1085.
(48) Kawahata, R.; Tsukuda, T.; Yagi, T.; Fuyuhiro, A.; Kaizaki, S. *J. Alloys Compd.* **2006**, *408*, 976–980.
(49) Morioka-Yonezawa, A.; Sakagami-Yoshida, N.; Fuyuhiro, A.; Kaizaki, S. *Inorg. Chim. Acta* **2008**, *361*, 3623–3630.
(50) Yoneda, K.; Adachi, K.; Nishio, K.; Yamasaki, M.; Fuyuhiro, A.; Katada, M.; Kaizaki, S.; Kawata, S. *Angew. Chem., Int. Ed.* **2006**, *45*, 5459–5461.
(51) Hou, J. Z.; Li, M.; Li, Z.; Zhan, S. Z.; Huang, X. C.; Li, D. *Angew. Chem., Int. Ed.* **2008**, *47*, 1711–1714.
(52) Ishikawa, R.; Nakano, M.; Fuyuhiro, A.; Takeuchi, T.; Kimura, S.; Kashiwagi, T.; Hagiwara, M.; Kindo, K.; Kaizaki, S.; Kawata, S. *Chem.—Eur. J.* **2010**, *16*, 11139–11144.
(53) Bera, M.; Aromi, G.; Wong, W. T.; Ray, D. *Chem. Commun.* **2006**, 671–673.
(54) Bermejo, M. R.; Gonzalez-Noya, A. M.; Pedrido, R. M.; Romero, M. J.; Vazquez, M. *Angew. Chem., Int. Ed.* **2005**, *44*, 4182–4187.
(55) Vazquez, M.; Bermejo, M. R.; Licchelli, M.; Gonzalez-Noya, A. M.; Pedrido, R. M.; Sangregorio, C.; Sorace, L.; Garcia-Deibe, A. M.; Satunartin, J. *Eur. J. Inorg. Chem.* **2005**, 3479–3490.
(56) Bermejo, M. R.; Gonzalez-Noya, A. M.; Martinez-Calvo, M.; Pedrido, R.; Romero, M. J.; Lopez, M. V. *Eur. J. Inorg. Chem.* **2008**, 3852–3863.
(57) Zhu, A. X.; Zhang, J. P.; Lin, Y. Y.; Chen, X. M. *Inorg. Chem.* **2008**, *47*, 7389–7395.
(58) Zhan, S. Z.; Li, M.; Hou, J. Z.; Ni, J.; Li, D.; Huang, X. C. *Chem.—Eur. J.* **2008**, *14*, 8916–8921.
(59) Saalfrank, R. W.; Low, N.; Trummer, S.; Sheldrick, G. M.; Teichert, M.; Stalke, D. *Eur. J. Inorg. Chem.* **1998**, 559–563.
(60) Baxter, P. N. W.; Lehn, J. M.; Baum, G.; Fenske, D. *Chem.—Eur. J.* **2000**, *6*, 4510–4517.
(61) Pedrido, R.; Lopez, M. V.; Sorace, L.; Gonzalez-Noya, A. M.; Cwiklinska, M.; Suarez-Gomez, V.; Zaragoza, G.; Bermejo, M. R. *Chem. Commun.* **2010**, *46*, 4797–4799.
(62) Bao, X.; Leng, J. D.; Meng, Z. S.; Lin, Z. J.; Tong, M. L.; Nihei, M.; Oshio, H. *Chem.—Eur. J.* **2010**, *16*, 6169–6174.
(63) Kessissoglou, D. P. *Coord. Chem. Rev.* **1999**, *185−6*, 837–858.
(64) Baca, S. G.; Stoeckli-Evans, H.; Ambrus, C.; Malinovskii, S. T.; Malaestean, I.; Gerbeleu, N.; Decurtins, S. *Polyhedron* **2006**, *25*, 3617–3627.
(65) Bhula, R.; Gainsford, G. J.; Weatherburn, D. C. *J. Am. Chem. Soc.* **1988**, *110*, 7550–7552.
(66) Ribas, J.; Albela, B.; StoeckliEvans, H.; Christou, G. *Inorg. Chem.* **1997**, *36*, 2352–2360.
(67) Kim, J.; Jin, M. L.; Dom, Y. *Eur. J. Inorg. Chem.* **2003**, 2563–2566.
(68) Viciano-Chumillas, M.; Gimenez-Marques, M.; Tanase, S.; Evangelisti, M.; Mutikainen, I.; Turpeinen, U.; Smits, J. M. M.; de Gelder, R.; de Jongh, L. J.; Reedijk, J. *J. Phys. Chem. C* **2008**, *112*, 20525–20534.
(69) Cano, J.; Cauchy, T.; Ruiz, E.; Milios, C. J.; Stoumpos, C. C.; Stamatatos, T. C.; Perlepes, S. P.; Christou, G.; Brechin, E. K. *Dalton Trans.* **2008**, 234–240.
(70) Lampropoulos, C.; Abboud, K. A.; Stamatatos, T. C.; Christou, G. *Inorg. Chem.* **2009**, *48*, 813–815.
(71) Viciano-Chumillas, M.; Tanase, S.; Mutikainen, I.; Turpeinen, U.; de Jongh, L. J.; Reedijk, J. *Inorg. Chem.* **2008**, *47*, 5919–5929.
(72) Maayan, G.; Christou, G. *Inorg. Chem.* **2011**, DOI: dx.doi.org/10.1021/ic200393y.
(73) *Data collection with APEX II v2009.1-02*; Bruker AXS Inc.: Madison, WI, USA, 2007.
(74) *Data reduction with Bruker SAINT V7.60A*; Bruker AXS Inc.: Madison, WI, USA, 2007.
(75) *SADABS: V2008/1*; Bruker AXS Inc.: Madison, WI, USA, 2001; Blessing, *Acta Crystallogr.* **1995**, *A51*, 33−38.
(76) Sheldrick, G. M. *Acta Crystallogr.* **2008**, *A64*, 112–122SHELXTL V6.14.
(77) Glerup, J.; Goodson, P. A.; Hodgson, D. J.; Michelsen, K.; Nielsen, K. M.; Wiehe, H. *Inorg. Chem.* **1992**, *31*, 4611–4616.
(78) Kostakis, G. E.; Powell, A. K. *Coord. Chem. Rev.* **2009**, *253*, 2686–2697.
(79) Sens, C.; Rodriguez, M.; Romero, I.; Llobet, A.; Parella, T.; Benet-Buchholz, J. *Inorg. Chem.* **2003**, *42*, 8385–8394.
(80) Sens, C.; Rodriguez, M.; Romero, I.; Llobet, A.; Parella, T.; Sullivan, B. P.; Benet-Buchholz, J. *Inorg. Chem.* **2003**, *42*, 2040–2048.
(81) Bard, A. J. *Pure Appl. Chem.* **1971**, *25*, 379–394.
(82) Ammar, F.; Saveant, J. M. *J. Electroanal. Chem.* **1973**, *47*, 115–125.
(83) Dunand-Sauthier, M.-N. C.; Deronzier, A.; Pradon, X.; Ménage, S.; Philouze, C. *J. Am. Chem. Soc.* **1997**, *119*, 3173–3174.
(84) Romain, S.; Duboc, C.; Neese, F.; Rivière, E.; Hanton, L. R.; Blackman, A. G.; Philouze, C.; Leprêtre, J.-C.; Deronzier, A.; Collomb, M.-N. *Chem.—Eur. J.* **2009**, *15*, 980–988.
(85) Romain, S.; Baffert, C.; Duboc, C.; Lepretre, J. C.; Deronzier, A.; Collomb, M. N. *Inorg. Chem.* **2009**, *48*, 3125–3131.
(86) Vincent, J. B.; Chang, H. R.; Folting, K.; Huffman, J. C.; Christou, G.; Hendrickson, D. N. *J. Am. Chem. Soc.* **1987**, *109*, 5703–5711.
(87) Brunold, T. C.; Gamelin, D. R.; Stemmler, T. L.; Mandal, S. K.; Armstrong, W. H.; Penner-Hahn, J. E.; Solomon, E. I. *J. Am. Chem. Soc.* **1998**, *120*, 8724–8738.
(88) Reynolds, R. A.; Yu, W. O.; Dunham, W. R.; Coucouvanis, D. *Inorg. Chem.* **1996**, *35*, 2721–2722.
(89) Duboc, C.; Collomb, M.-N.; Pécaut, J.; Deronzier, A.; Neese, F. *Chem.—Eur. J.* **2008**, *14*, 6498–6509.
(90) Rich, J.; Castillo, C. E.; Romero, I.; Rodriguez, M.; Duboc, C.; Collomb, M. N. *Eur. J. Inorg. Chem.* **2010**, 3658–3665.
(91) Duboc, C.; Collomb, M. N.; Neese, F. *Appl. Magn. Reson.* **2010**, *37*, 229–245.
(92) Baffert, C.; Dumas, S.; Chauvin, J.; Leprêtre, J.-C.; Collomb, M.-N.; Deronzier, A. *Phys. Chem. Chem. Phys.* **2005**, *7*, 202–210.
(93) Romain, S.; Baffert, C.; Dumas, S.; Chauvin, J.; Leprêtre, J.-C.; Daveloose, D.; Deronzier, A.; Collomb, M.-N. *Dalton Trans.* **2006**, 5691–5702.
(94) van Vleck, J. H. *The Theory of Electric and Magnetic Susceptibility*; Oxford University Press: New York, 1932.
(95) Kambe, K. *J. Phys. Soc. Jpn.* **1950**, *5*, 48–51.
(96) To take into account the interactions between complexes, the following definition of the susceptibility has been used:

$$\chi = \frac{\chi_{\text{complex}}}{1 - \dfrac{2zJ'}{Ng^2\mu_B^2}\chi_{\text{complex}}}$$

see for example: (a) Myers, B. E.; Berger, L.; Friedberg, S. *J. Appl. Phys.* **1969**, *40*, 1149–1151. (b) O'Connor, C. J. *Prog. Inorg. Chem.* **1982**, *29*, 203–283.